THE JOURNAL OF PHYSICAL CHEMISTRY LETTERS
A JOURNAL OF THE AMERICAN CHEMICAL SOCIETY

pubs.acs.org/JPCL Letter

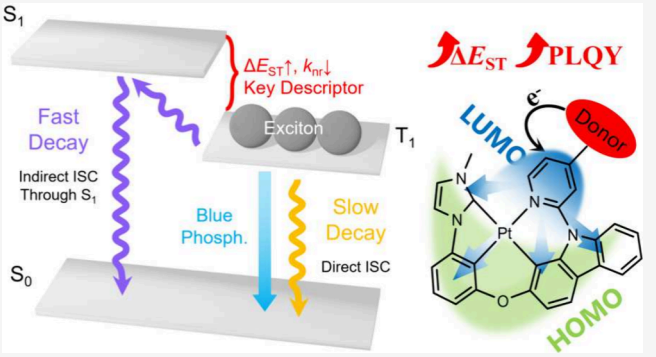
# Multi-channel Non-radiative Dynamics to Reveal $\Delta E_{ST}$ as the Key Efficiency Descriptor for Deep-Blue Pt(II) Phosphors

Xiao Chen, Weitang Li, Wenjie Zhang, Yulong Li, Yaxin Wang, and Zhigang Shuai*

Cite This: J. Phys. Chem. Lett. 2026, 17, 12289−12296 Read Online

ACCESS | Metrics & More | Article Recommendations | Supporting Information

**ABSTRACT:** Tetradentate platinum(II) complexes are promising candidates for phosphorescent organic light-emitting diodes (OLEDs), combining deep-blue emission, high color purity, and potential for near-unity photoluminescence quantum yields (PLQYs). However, despite their rigid structures, which should suppress non-radiative decay, many of these complexes still show surprisingly low PLQYs, and the mechanism underlying this discrepancy has remained unclear. Here, through first-principle calculations of multi-channel transition rates for 25 tetradentate Pt(II) complexes, we show that this apparent paradox arises from a thermally activated $S_1$ non-radiative channel ($T_1 \rightarrow S_1 \rightarrow S_0$) that dominates the non-radiative decay. The rate of this channel depends exponentially on the singlet−triplet gap $\Delta E_{ST}$, establishing $\Delta E_{ST}$ as a key descriptor for PLQY. Electronic structural analysis reveals that donors on the pyridine unit can delocalize LUMO, increase HOMO−LUMO overlap, and help enlarge $\Delta E_{ST}$ and PLQY. These results provide a unified mechanistic picture and a direct design rule for high-efficiency deep-blue Pt(II) emitters.

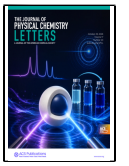



Organic light-emitting diodes (OLEDs) are widely used devices with promising prospects for further development.[1−4] As a core component, light-emitting materials have undergone several generations of evolution over the decades, and new materials with superior properties continue to be synthesized and reported.[5−7] Among them, heavy-metal complexes, particularly those based on platinum and iridium, constitute a notably important class.[8−17] Owing to the strong spin−orbit coupling (SOC) arising from heavy atoms, these molecules can convert singlet excitons to triplets via intersystem crossing (ISC) and subsequently emit phosphorescence, achieving a theoretical photoluminescence quantum yield (PLQY) of up to 100%. While green- and red-emitting materials of this type have already been commercialized, blue-emitting molecules have long faced development challenges, primarily due to stability issues.[5] Furthermore, poor color purity remains a common problem associated with these phosphorescent emitters.

In 2014, Li et al. achieved a breakthrough with the synthesis of PtON7 and PtON7-dtb.[18] These two tetradentate Pt complexes exhibit high rigidity, and minimal structural relaxation results in a spectral full width at half maximum (fwhm) of only 20 nm. In 2022, two blue-emitting molecules with similar structures, BD-01 and BD-02, were reported, demonstrating a device lifetime exceeding 1000 h and narrow emission spectra.[19] Inspired by these advances, over 100 new molecules of this type have been synthesized and reported over the past decade, many of which exhibit excellent properties, such as high color purity and prolonged device lifetime.[20−28] Collectively, these findings underscore the immense potential of tetradentate platinum complexes as blue OLED materials.

Unfortunately, many such molecules exhibit surprisingly low PLQYs, which has become a key factor limiting the application and development of these materials.[29−31] In general, PLQY depends on the relative magnitudes of radiative and non-radiative decay rates ($k_{nr}$), with the intersystem crossing from $T_1$ to $S_0$ typically considered the primary pathway for non-radiative processes in phosphorescent materials. However, the rigid structure of the tetradentate Pt complexes results in very small Huang−Rhys factors,[32,33] which significantly suppress the direct ISC process. Therefore, this pathway alone is insufficient to account for the large non-radiative rates observed in molecules with low PLQYs. Some researchers have proposed that the minimum energy crossing point (MECP) plays a significant role, but this remains controversial.[34−38] Due to a limited understanding of the mechanisms underlying non-radiative transitions, there is a theoretical lack of effective descriptors for PLQY and,

Received: September 23, 2026
Revised: October 9, 2026
Accepted: October 12, 2026
Published: October 16, 2026



Downloaded from pubs.acs.org/jpclcd/article-pdf/17/43/12289/6888372/acs.jpclett.6c03198.pdf by CHINESE UNIV OF HONG KONG SHENZHEN user on 02 November 2026


© 2026 American Chemical Society

https://doi.org/10.1021/acs.jpclett.6c03198
J. Phys. Chem. Lett. 2026, 17, 12289−12296

consequently, a lack of targeted structural design strategies to experimentally enhance PLQY.

In this work, the radiative and non-radiative transition rates of 25 tetradentate Pt complexes are calculated, taking into account four non-radiative decay channels: (a) direct ISC from $T_1$ to $S_0$, (b) ISC from $T_2$ to $S_0$, (c) internal conversion (IC) from $S_1$ to $S_0$, and (d) MECP pathway. By a comparison of the results to experimantal values, it is found that the $S_1$ channel accounts for the majority of the non-radiative transition rates and that the rate of this process is strongly dependent on the magnitude of $\Delta E_{ST}$. Consequently, $\Delta E_{ST}$ can serve as an effective descriptor for both the non-radiative transition rate and the PLQY for this class of molecules. Furthermore, electronic structural analysis reveals that electron-donating substituents on the pyridine ring promote HOMO−LUMO overlap, thereby increasing $\Delta E_{ST}$ and enhancing PLQY. This work elucidates the mechanism underlying non-radiative transitions in tetradentate Pt complexes and provides rational design strategies for achieving high PLQY, which will contribute to the development of high-performance OLED materials.

The 25 tetradentate Pt(II) complexes examined in this study are all previously reported compounds. They share four kinds of skeletons, as shown in Figure 1, while their specific

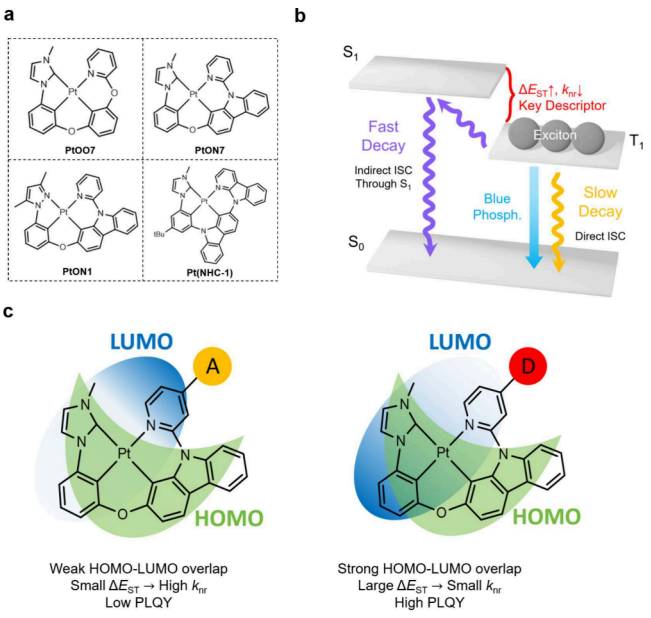



**Figure 1.** (a) Skeletons of the molecules studied in this work. (b) Diagram of the non-radiative transition mechanism. (c) Mechanism by which molecular structure influences PLQY.

structures are given in Figure S1. In our previous work, we found that density functional theory (DFT) and time-dependent DFT (TDDFT) using TPSSh give rather good predictions for the emission energies, and the spectra shape provided by TPSSh along with the thermally vibrational correlation function (TVCF) method agree well with experiments.[39] This (TD-)DFT + TVCF approach is not only universal and efficient but also capable of accurately determining the transition rate constant, and a carefully chosen functional could serve as a crucial guarantee for the reliability of results. Therefore, TPSSh/def2svp[40−44] in Gaussian 16[45] is used for all structure optimization and frequency analysis in this work. The SOCs, phosphorescent transition dipole moments, and MECPs are obtained using ORCA6.0,[46] and Multiwfn[47] is used for electronic structural analysis. For details of the calculation, please see the Supporting Information.

The four non-radiative transition channels considered in this work are shown in Figure 2. The transition rate constant of the

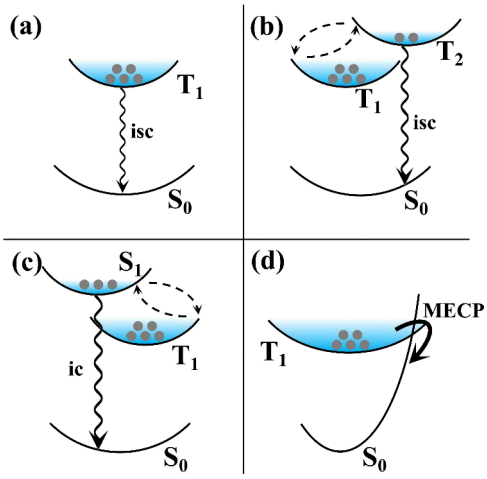



**Figure 2.** Four non-radiative transition channels considered in this work. (a) $T_1$ channel: direct ISC from $T_1$ to $S_0$. (b) $T_2$ channel: thermally activated reverse IC from $T_1$ to $T_2$ followed by ISC from $T_2$ to $S_0$. (c) $S_1$ channel: thermally activated reverse ISC from $T_1$ to $S_1$ followed by IC from $S_1$ to $S_0$. (d) MECP channel: non-radiative decay from MECP between $T_1$ and $S_0$.

MECP channel is evaluated via the transition state theory Erying equation as[48,49]

$$k_{nr}(\mathrm{MECP}) = \frac{k_B T}{h} e^{-\Delta E/k_B T} \quad (1)$$

where $\Delta E$ denotes the electronic energy gap between MECP and $T_1$ minimum, $k_B$ is Boltzmann's constant, $h$ is Planck's constant, and $T$ is the temperature ($T$ = 300 K unless otherwise stated). This assumes no other barriers between MECP and $T_1$ minimum and, thus, serves as an upper bound of true transition rates. The other transition rates are calculated using the TVCF method in MOMAP, which features very low computational complexity and introduces no truncation error for vibrational states.[50−53] The transition between excited states is very fast due to large SOCs and small energy gaps; therefore, the population of all excited states is approximately considered using the Boltzmann distribution. The effective transition rate constants for the $S_1$ channel and $T_2$ channel are thus given by

$$k_{nr}(S_1) = \frac{1}{3} e^{(E(T_1)) - E(S_1)/k_B T} k_{ic}(S_1) \quad (2)$$

$$k_{nr}(T_2) = e^{(E(T_1)) - E(T_2)/k_B T} k_{isc}(T_2) \quad (3)$$

where $k_{ic}$ and $k_{isc}$ are the direct transition rates and all $E$ denote adiabatic energy. The sum of transition rates of all four channels gives the total non-radiative transition rates, and with the phosphorescence rate $k_{phos}$, the PLQY is then calculated as

$$k_{nr} = k_{isc}(T_1) + k_{nr}(\mathrm{MECP}) + k_{nr}(S_1) + k_{nr}(T_2) \quad (4)$$



https://doi.org/10.1021/acs.jpclett.6c03198
J. Phys. Chem. Lett. 2026, 17, 12289−12296

Downloaded from pubs.acs.org/jpclcd/article-pdf/17/43/12289/6888372/acs.jpclett.6c03198.pdf by CHINESE UNIV OF HONG KONG SHENZHEN user on 02 November 2026

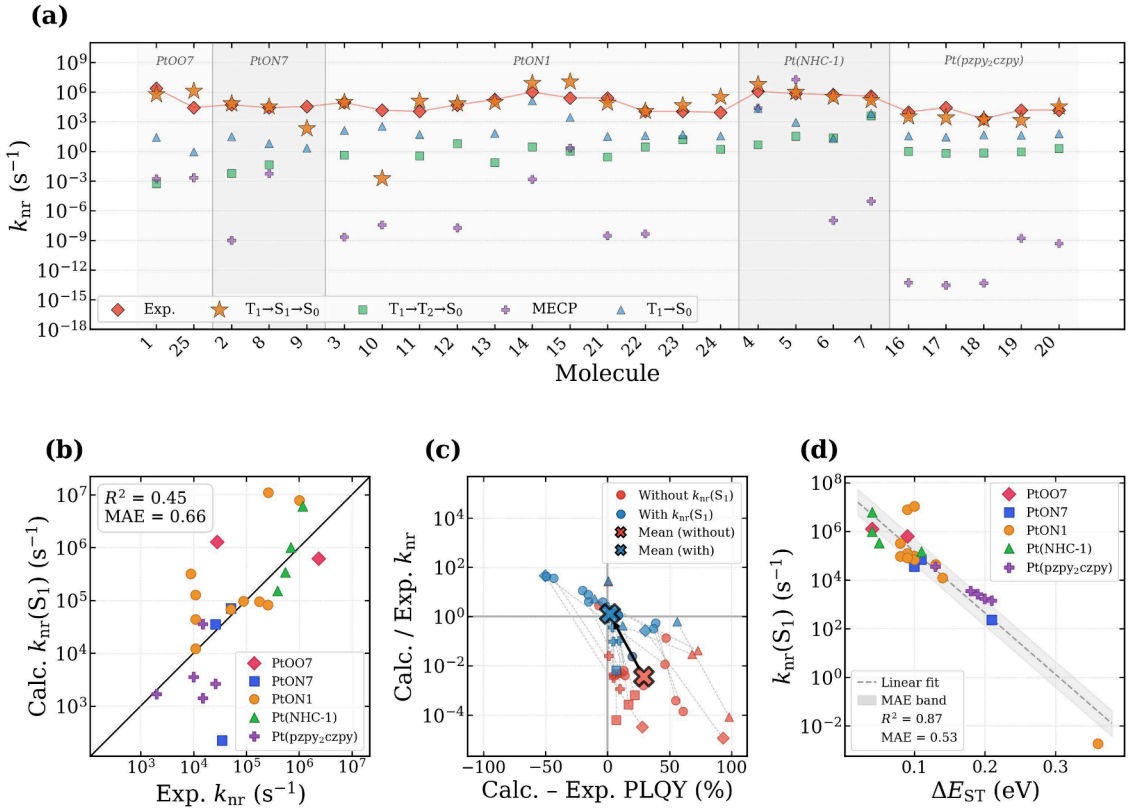



**Figure 3.** (a) Calculated and experimental non-radiative transition rates. (b) Scatter plot of calculated rates for the $S_1$ channel against experimental non-radiative rates. Molecule **10** is omitted due to too small $k_{nr}(S_1)$. (c) Error of non-radiative rates and PLQY, with or without consideration of the $S_1$ channel. (d) Scatter plot of calculated $S_1$ channel rates and $\Delta E_{ST}$.

$$\text{PLQY} = \frac{k_{phos}}{k_{phos} + k_{nr}} \tag{5}$$

The calculated non-radiative rate constants are presented in Figure 3 alongside the corresponding experimental $k_{nr}$ values. Among the four channels considered, the MECP pathway yields the smallest rates for most molecules, owing to the high energy barriers, typically ranging from 0.9 to 1.5 eV. Only molecule **5** exhibits a relatively low energy barrier of 0.33 eV, for which the MECP contribution to the non-radiative rate could be non-negligible. Given that the rates calculated under no barrier assumption represent an upper bound of true transition rates, the MECP contribution can, in general, be reasonably neglected. The rates derived from the $T_2$ channel are also very small, all falling at least 2 orders of magnitude below the experimental values. Although the SOCs between the $T_2$ and $S_0$ states are as large as approximately 100 $cm^{-1}$, the energy gaps between $T_1$ and $T_2$ exceed 0.2 eV in most cases, resulting in a low $T_2$ population and transition rates. With regard to the direct ISC from $T_1$ to $S_0$, the calculated rates are generally several orders of magnitude lower than the experimental values, with molecules **12** and **14** being the only exceptions. As anticipated from the narrow emission spectra of these molecules, the small structural relaxation indeed inhibits effective direct ISC. As shown in the scatter plots in Figure S2, not only are the results of the above three channels generally much smaller than the experimental values, but they also exhibit very poor correlation with them. Therefore, these channels are unlikely to play a significant role in the non-radiative transitions of these molecules.

In contrast, the $S_1$ channel contributes the largest non-radiative rate for most molecules, and the calculated values are generally close to the experimental $k_{nr}$ values, with molecule **10** being the only exception. In molecule **10**, the $S_1$ state lies 0.36 eV above $T_1$, a significantly larger energy gap compared to the $\Delta E_{ST}$ values of the other molecules, resulting in a very low $S_1$ population and a negligible transition rate. As shown in Figure 3b, the calculated rates exhibit a good correlation with the experimental data. We further calculated the PLQY of these molecules both with and without considering the $S_1$ channel. As illustrated in Figure 3c, the calculated $k_{nr}$ without the $S_1$ channel component is significantly smaller than the experiment, and the PLQY is overall too large. When the $S_1$ pathway is included, the results become much closer to the experiment, with their mean value almost identical. These results indicate that the $S_1$–$S_0$ transition plays a dominant role in the non-radiative processes of tetradentate Pt complexes.

Given that the $S_1$ channel governs the total non-radiative rates, identifying the key parameter that reflects its magnitude is of critical importance. Since the molecules share similar skeletons, their vibrational properties and direct internal conversion rates from $S_1$ to $S_0$ are likely to differ only marginally. Consequently, the Boltzmann population of the $S_1$ state and, thus, $\Delta E_{ST}$ may serve as the decisive variable. As shown in Figure 3d, a strong linear relationship exists between the logarithm of the calculated rates and $\Delta E_{ST}$, indicating that $\Delta E_{ST}$ serves as an excellent descriptor for the $k_{nr}$ values of tetradentate Pt complexes. Typically, a $\Delta E_{ST}$ of approximately 0.1 eV is associated with a non-radiative rate of around $10^5$ $s^{-1}$ and a low PLQY. In contrast, a $\Delta E_{ST}$ of 0.15 eV or larger leads



https://doi.org/10.1021/acs.jpclett.6c03198
J. Phys. Chem. Lett. 2026, 17, 12289−12296

Downloaded from pubs.acs.org/jpclcd/article-pdf/17/43/12289/6888372/acs.jpclett.6c03198.pdf by CHINESE UNIV OF HONG KONG SHENZHEN user on 02 November 2026

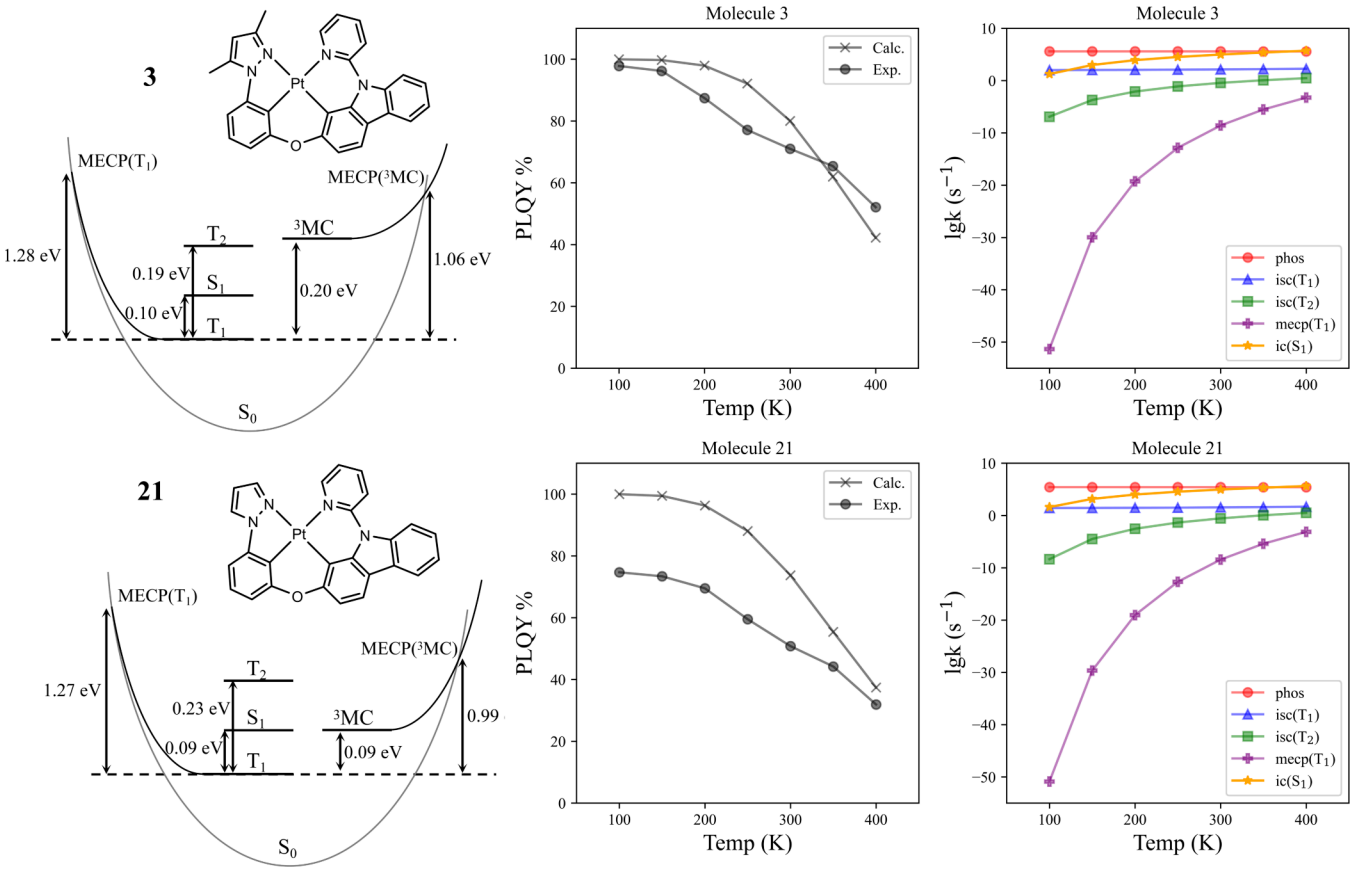



**Figure 4.** Structure, energy diagram, and temperature dependence of rates and PLQY for molecules **3** and **21**.

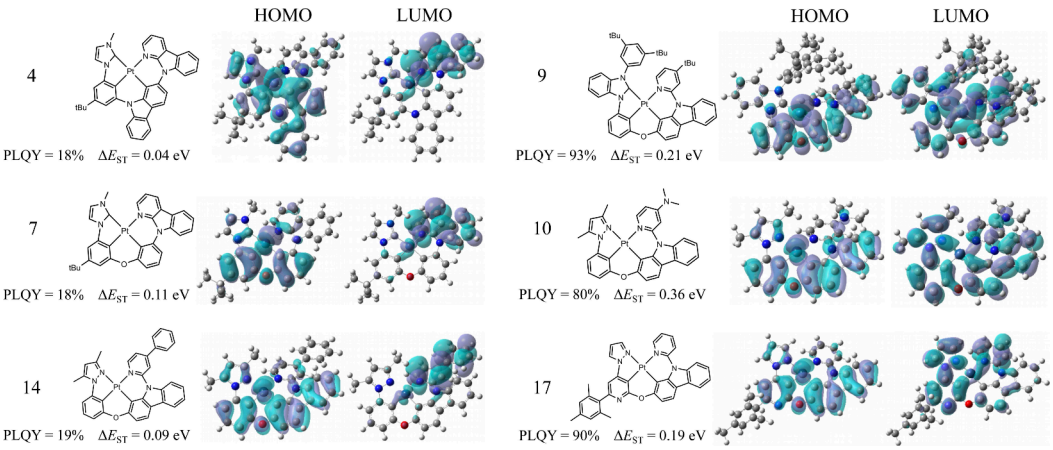



**Figure 5.** Structure, experimental PLQY, calculated $\Delta E_{ST}$, and frontier orbitals of the molecules.

to negligible non-radiative rates and a PLQY approaching unity.

To gain a deeper understanding of the non-radiative transition mechanism in tetradentate Pt complexes, the temperature dependence of the transition rates and PLQY was calculated for molecules **3** and **21**. In addition to the four non-radiative channels discussed earlier, we also considered the MECP between $S_0$ and the metal-centered triplet state ($^3$MC), which has been suggested in some studies as a potential contributor to non-radiative transitions.[37,54−58] Optimizing the $^3$MC state is particularly challenging due to its highly twisted structure and relatively shallow potential well. Nevertheless, we successfully located the equilibrium structures for these two molecules using the method described in ref 59. A large displacement along the dihedral angle between the pyridine and carbazole moieties is observed, consistent with previous reports.[32,60]

As shown in Figure 4, the MECPs all possess very high energies, in agreement with previous reports.[32,35,38,49,60] Consequently, the transition rates arising from the MECP pathway are negligible across the entire temperature range studied here. The $S_1$ states are significantly lower in energy than the $T_2$ states, and given that internal conversion is typically several orders of magnitude faster than intersystem crossing, the rates contributed by the $T_2$ channel are also negligible compared to those from the $S_1$ channel. In contrast,



https://doi.org/10.1021/acs.jpclett.6c03198
J. Phys. Chem. Lett. 2026, 17, 12289−12296

Downloaded from pubs.acs.org/jpclcd/article-pdf/17/43/12289/6882372/acs.jpclett.6c03198.pdf by CHINESE UNIV OF HONG KONG SHENZHEN user on 02 November 2026

the phosphorescence rate and the direct ISC rate from $T_1$ are not sensitive to the temperature, rendering the latter comparable to the $S_1$ channel rate at low temperatures, where the population of $S_1$ decreases dramatically. The calculated PLQY for molecule **3** shows excellent agreement with the experimental value. For molecule **21**, the calculated PLQY is slightly higher than the experimental value due to a slight overestimation of the phosphorescence rate, but they show the same trend. These results further confirm that the $S_1$ channel makes the dominant contribution to the non-radiative transitions of tetradentate Pt complexes.

In the preceding subsections, we have established that the $S_1$ channel constitutes the most important pathway for non-radiative transitions in tetradentate Pt complexes and that $\Delta E_{ST}$ is a key parameter governing the rate of this process. To explore the relationship between the molecular structure and $\Delta E_{ST}$, the frontier orbitals of six representative molecules are plotted in Figure 5. Regardless of PLQY, the HOMO of these molecules is predominantly distributed over the benzene and carbazole moieties. In contrast, the distribution of the LUMO varies significantly with PLQY. In molecules with lower PLQY, the LUMO is largely localized on the pyridine ring and its substituents. In molecules with higher PLQY, however, the LUMO exhibits substantially greater delocalization, extending across most regions of the molecule, including the pyridine, benzene, and diazole units. Given that $\Delta E_{ST}$ is approximately positively correlated with the degree of HOMO−LUMO overlap,[61,62] differences in the LUMO distribution clearly represent a direct factor contributing to the variation in $\Delta E_{ST}$ among these molecules.

Specifically, because pyridine is the strongest electron-withdrawing moiety in the molecule, the LUMO generally tends to localize on it. In molecules where the pyridine ring bears conjugated substituents (e.g., molecules **4**, **7**, and **14**), the LUMO, localized on the pyridine ring, becomes spatially separated from the HOMO, resulting in a relatively limited HOMO−LUMO overlap and a small $\Delta E_{ST}$. Conversely, when electron-donating substituents are attached to the pyridine (e.g., molecules **9** and **10**), these groups weaken the electron-withdrawing character of the pyridine, thereby pushing the LUMO away from the pyridine and distributing it over other parts of the molecule. Once this occurs, the LUMO can overlap more extensively with the HOMO, leading to a large $\Delta E_{ST}$. This effect intensifies with an increasing electron-donating strength of the substituent: for a weak donor, such as *tert*-butyl, $\Delta E_{ST}$ increases only modestly, whereas a strong donor, such as dimethylamino, can raise $\Delta E_{ST}$ to such an extent that the $S_1$ channel no longer contributes appreciably to non-radiative transitions. In the absence of substituents on pyridine, $\Delta E_{ST}$ and PLQY are governed by other structural features and can be either high (e.g., molecules **18** and **19**) or low (e.g., molecules **1** and **21**).

To further investigate the influence of the molecular structure on PLQY, a series of new molecules are designed and their PLQY values are calculated, with the results presented in Figure 6. These molecules are based on PtNO1 and PtON7 skeletons, with substituents of varying electronic character attached to pyridine, ranging from strong acceptors, such as $-NO_2$ and $-CF_3$, to strong donors, like alkoxy and tetrahydropyrrole. As established in the preceding analysis, the PLQY increases with the electron-donating strength of the substituents. Acceptors further localize the LUMO onto the pyridine ring, leading to limited HOMO−LUMO overlap and

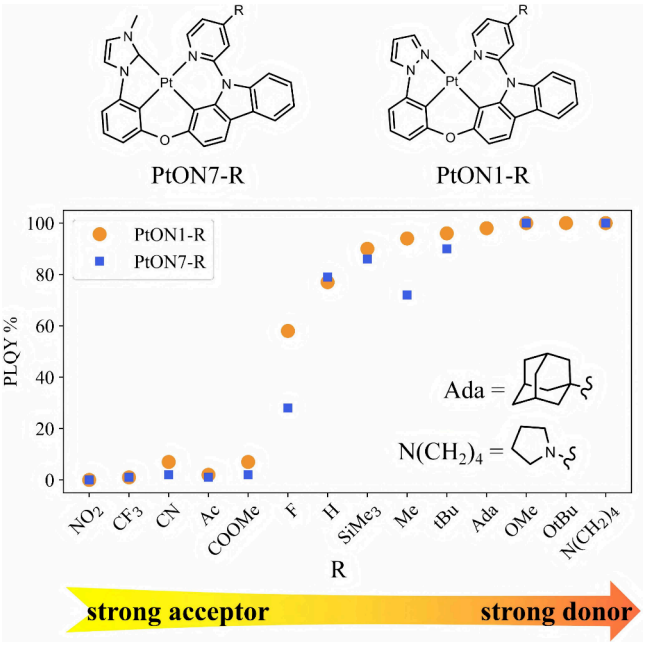



**Figure 6.** Structures and calculated PLQY of the designed molecules. Here, only the rates of the $S_1$ channel are considered in $k_{nr}$.

a small $\Delta E_{ST}$, thereby resulting in a PLQY close to zero. In contrast, donors produce the opposite effect, yielding a PLQY approaching unity. A dramatic change in PLQY from 0 to 1 occurs when the substituent exerts an electronic effect comparable to that of a hydrogen atom, i.e., in the absence of a substituent. At this juncture, PLQY becomes highly sensitive to the molecular structure, a finding consistent with the conclusions drawn from the analysis of the 25 molecules. In summary, to achieve high luminescence efficiency in this class of molecules, it is advisible to attach electron-donating groups to the pyridine ring.

The radiative and non-radiative transition rate constants along four different channels are calculated for 25 tetradentate Pt complexes, and the results are compared to corresponding experiments. Among these channels, the pathway involving reverse intersystem crossing from $T_1$ to $S_1$ followed by internal conversion from $S_1$ to $S_0$ is identified as the most significant. This finding is further supported by an analysis of the temperature dependence of the transition rates and PLQY. Moreover, $\Delta E_{ST}$ exhibits a clear correlation with the non-radiative rates and, therefore, serves as a reliable descriptor for PLQY. Through detailed electronic structural analysis and additional validation calculations, we demonstrate that attaching an electron-donating group to the pyridine ring enhances HOMO−LUMO overlap and increases $\Delta E_{ST}$, thereby reducing the population of the $S_1$ state and the non-radiative transition rate, ultimately leading to a PLQY approaching unity. This work is expected to inform the rational design of high-performance Pt-based phosphorescent materials and to contribute to the advancement of OLED development.

## ■ ASSOCIATED CONTENT

### Supporting Information

The Supporting Information is available free of charge at https://pubs.acs.org/doi/10.1021/acs.jpclett.6c03198.

Downloaded from pubs.acs.org/jpclcd/article-pdf/17/43/12289/6888372/acs.jpclett.6c03198.pdf by CHINESE UNIV OF HONG KONG SHENZHEN user on 02 November 2026



https://doi.org/10.1021/acs.jpclett.6c03198
J. Phys. Chem. Lett. 2026, 17, 12289−12296

Optimized coordinates for $S_0$, $S_1$, $T_1$, $T_2$, and MECP (ZIP)

Details of the calculation method, molecular structures, tables of calculated and experimental data, and scatter plots of calculated rates against experiments (PDF)

## AUTHOR INFORMATION


### Corresponding Author

**Zhigang Shuai** − *Department of Chemistry, MOE Key Laboratory of Organic OptoElectronics and Molecular Engineering, Tsinghua University, Beijing 100084, China; Guangdong Basic Research Center of Excellence for Aggregate Science, School of Science and Engineering, The Chinese University of Hong Kong, Shenzhen, Guangdong 518172, China;* orcid.org/0000-0003-3867-2331; Email: shuaizhigang@cuhk.edu.cn

### Authors

**Xiao Chen** − *Department of Chemistry, MOE Key Laboratory of Organic OptoElectronics and Molecular Engineering, Tsinghua University, Beijing 100084, China;* orcid.org/0009-0004-4824-5928

**Weitang Li** − *Guangdong Basic Research Center of Excellence for Aggregate Science, School of Science and Engineering, The Chinese University of Hong Kong, Shenzhen, Guangdong 518172, China;* orcid.org/0000-0002-8739-641X

**Wenjie Zhang** − *Department of Chemistry, MOE Key Laboratory of Organic OptoElectronics and Molecular Engineering, Tsinghua University, Beijing 100084, China;* orcid.org/0009-0003-2392-7992

**Yulong Li** − *Guangdong Basic Research Center of Excellence for Aggregate Science, School of Science and Engineering, The Chinese University of Hong Kong, Shenzhen, Guangdong 518172, China*

**Yaxin Wang** − *Guangdong Basic Research Center of Excellence for Aggregate Science, School of Science and Engineering, The Chinese University of Hong Kong, Shenzhen, Guangdong 518172, China*

Complete contact information is available at: https://pubs.acs.org/10.1021/acs.jpclett.6c03198


### Notes

The authors declare no competing financial interest.

## ACKNOWLEDGMENTS

The authors thank the National Natural Science Foundation of China (Grants T2350009 and 22433007), the Guangdong Provincial Natural Science Foundation (Grant 2024A1515011185), and the Shenzhen City Peacock Team Project (Grant KQTD20240729102028011). The authors also acknowledge support from the Young Scientists Fund of the National Natural Science Foundation of China (NSFC, Grant 22503077) and the China Postdoctoral Science Foundation (Grant 2025M771052).

## REFERENCES


(1) Zhou, H.; et al. Exciplex-enabled high-efficiency, fully stretchable OLEDs. *Nature* **2026**, *649*, 604.

(2) Joo, W.-J.; Kyoung, J.; Esfandyarpour, M.; Lee, S.-H.; Koo, H.; Song, S.; Kwon, Y.-N.; Song, S. H.; Bae, J. C.; Jo, A.; Kwon, M.-J.; Han, S. H.; Kim, S.-H.; Hwang, S.; Brongersma, M. L. Metasurface-driven OLED displays beyond 10,000 pixels per inch. *Science* **2020**, *370*, 459.

(3) Kim, M.; Kim, J.; Yoo, S. Near-planar light outcoupling structures with finite lateral dimensions for ultra-efficient and optical crosstalk-free OLED displays. *Nat. Commun.* **2025**, *16*, 8.

(4) Forrest, S. R. The path to ubiquitous and low-cost organic electronic appliances on plastic. *Nature* **2004**, *428*, 911−918.

(5) Hong, G.; Gan, X. M.; Leonhardt, C.; Zhang, Z.; Seibert, J.; Busch, J. M.; Bräse, S. A Brief History of OLEDs—Emitter Development and Industry Milestones. *Adv. Mater.* **2021**, *33*, 24.

(6) Yuan, G.; Wang, Y.-C.; Zhang, Z.; Liu, J.-Y.; He, Y.-H.; Chen, G.-W.; Li, Y.-Q.; Tang, J.-X. Complementarity fusion of boron−oxygen and carbazole blocks enables narrowband blue OLEDs with high performance. *Nat. Commun.* **2025**, *16*, 11.

(7) Mamada, M.; Kataoka, K.; Ochi, J.; Lee, T.; Matsumoto, R.; Yoshioka, M.; Fukushima, D.; Hatakeyama, T. Organic spontaneous emission approaching the monochromatic limit. *Science* **2026**, *392*, 1148−1153.

(8) Lamansky, S.; Djurovich, P.; Murphy, D.; Abdel-Razzaq, F.; Lee, H. E.; Adachi, C.; Burrows, P. E.; Forrest, S. R.; Thompson, M. E. Highly phosphorescent bis-cyclometalated iridium complexes: Synthesis, photophysical characterization, and use in organic light emitting diodes. *J. Am. Chem. Soc.* **2001**, *123*, 4304−4312.

(9) Lee, J.; Chen, H.-F.; Batagoda, T.; Coburn, C.; Djurovich, P. I.; Thompson, M. E.; Forrest, S. R. Deep blue phosphorescent organic light-emitting diodes with very high brightness and efficiency. *Nat. Mater.* **2016**, *15*, 92.

(10) Tuong Ly, K.; Chen-Cheng, R.-W.; Lin, H.-W.; Shiau, Y.-J.; Liu, S.-H.; Chou, P.-T.; Tsao, C.-S.; Huang, Y.-C.; Chi, Y. Near-infrared organic light-emitting diodes with very high external quantum efficiency and radiance. *Nat. Photonics* **2017**, *11*, 63−68.

(11) Yang, X. L.; Guo, H. R.; Liu, B.; Zhao, J.; Zhou, G. J.; Wu, Z. X.; Wong, W.-Y. Diarylboron-Based Asymmetric Red-Emitting Ir(III) Complex for Solution-Processed Phosphorescent Organic Light-Emitting Diode with External Quantum Efficiency above 28%. *Advanced Science* **2018**, *5*, 1701067.

(12) Soellner, J.; Strassner, T. Phosphorescent Cyclometalated Platinum(II) aNHC Complexes. *Chem. - Eur. J.* **2018**, *24*, 15603−15612.

(13) Wang, L.; Miao, J. S.; Zhang, Y. M.; Wu, C. J.; Huang, H.; Wang, X. Z.; Yang, C. L. Discrete Mononuclear Platinum(II) Complexes Realize High-Performance Red Phosphorescent OLEDs with EQEs of up to 31.8% and Superb Device Stability. *Adv. Mater.* **2023**, *35*, 9.

(14) Yang, X. L.; Xu, X. B.; Zhao, J.; Dang, J. S.; Huang, Z.; Yan, X. G.; Zhou, G. J.; Wang, D. D. Phosphorescent Platinum(II) Complexes Bearing 2-Vinylpyridine-type Ligands: Synthesis, Electrochemical and Photophysical Properties, and Tuning of Electrophosphorescent Behavior by Main-Group Moieties. *Inorg. Chem.* **2014**, *53*, 12986−13000.

(15) Li, B. N.; Li, Y. G.; Chan, M. H. Y.; Yam, V. W. W. Phosphorescent Cyclometalated Platinum(II) Enantiomers with Circularly Polarized Luminescence Properties and Their Assembly Behaviors. *J. Am. Chem. Soc.* **2021**, *143*, 21676−21684.

(16) Fecková, M.; Kahlal, S.; Roisnel, T.; Saillard, J. Y.; Boixel, J.; Hruzd, M.; le Poul, P.; Gauthier, S.; Robin-le Guen, F.; Bures, F.; Achelle, S. Cyclometallated 2-Phenylpyrimidine Derived Platinum Complexes: Synthesis and Photophysical Properties. *Eur. J. Inorg. Chem.* **2021**, *2021*, 1592−1600.

(17) Zhu, Z.-Q.; Klimes, K.; Holloway, S.; Li, J. Efficient Cyclometalated Platinum(II) Complex with Superior Operational Stability. *Adv. Mater.* **2017**, *29*, 5.

(18) Fleetham, T.; Li, G. J.; Wen, L. L.; Li, J. Efficient "Pure" Blue OLEDs Employing Tetradentate Pt Complexes with a Narrow Spectral Bandwidth. *Adv. Mater.* **2014**, *26*, 7116.

(19) Sun, J.; Ahn, H.; Kang, S.; Ko, S.-B.; Song, D.; Um, H. A.; Kim, S.; Lee, Y.; Jeon, P.; Hwang, S.-H.; You, Y.; Chu, C.; Kim, S. Exceptionally stable blue phosphorescent organic light-emitting diodes. *Nat. Photonics* **2022**, *16*, 212.


Downloaded from pubs.acs.org/jpclcd/article-pdf/17/43/12289/6888372/acs.jpclett.6c03198.pdf by CHINESE UNIV OF HONG KONG SHENZHEN user on 02 November 2026

(20) Jung, Y. H.; Lee, G. S.; Murugananthan, S.; Kim, H. R.; Oh, J. H.; Ham, J. H.; Yadav, S. B.; Lee, J. H.; Chae, M. Y.; Kim, Y.-H.; Kwon, J. H. Modified *t*-butyl in tetradentate platinum(II) complexes enables exceptional lifetime for blue-phosphorescent organic light-emitting diodes. *Nat. Commun.* **2024**, *15*, 11.
(21) Li, G. J.; Chu, Q. S.; Yao, H. H.; Wu, K. W.; She, Y. B. High-performance deep-blue phosphorescent organic light-emitting diodes enabled by a platinum(ii) emitter. *Nat. Photonics* **2025**, *19*, 977−984.
(22) Kim, J. M.; Cheong, K.; Jiang, J. X.; Jeon, S. O.; Hong, W. P.; Lee, J. Y. Tetradentate Pt complexes for organic light-emitting diodes. *Trends in Chemistry* **2023**, *5*, 267−278.
(23) You, Y. Pt(II) complexes with tetradentate ligands: Toward commercially applicable blue organic electroluminescence devices. *Coord. Chem. Rev.* **2025**, *526*, 216374.
(24) Fleetham, T.; Li, G. J.; Wen, L. L.; Li, J. Efficient "Pure" Blue OLEDs Employing Tetradentate Pt Complexes with a Narrow Spectral Bandwidth. *Adv. Mater.* **2014**, *26*, 7116.
(25) Hang, X. C.; Fleetham, T.; Turner, E.; Brooks, J.; Li, J. Highly Efficient Blue-Emitting Cyclometalated Platinum(II) Complexes by Judicious Molecular Design. *Angew. Chem., Int. Ed.* **2013**, *52*, 6753−6756.
(26) Xu, K. W.; Zhang, C. Y.; Yang, L. P.; Zhan, F.; Lou, W. W.; Yang, Y.-F.; She, Y. B.; Li, G. J. Molecular Engineering of a Rigid Tetradentate Pt(II) Emitter for High-Performance OLEDs Realizing the BT.2020 Blue Gamut. *Angew. Chem., Int. Ed.* **2025**, *64*, 13.
(27) Zhang, C. Y.; Xu, K. W.; Yang, Y.-F.; She, Y. B.; Li, G. J. Dual Regulation of Molecular Rigidity and Orbital Engineering of Pt(II) Emitters for High-Performance Deep-Blue OLEDs. *Advanced Science* **2025**, *12*, 10.
(28) Zhu, J. N.; Huang, M. L.; Zhang, Y. M.; Chen, Z. X.; Deng, Y. J.; Zhang, H. Y.; Wang, X. Z.; Yang, C. L. Improving the Blue Color Purity of Tetradentate Pt(II) Complexes with the Assistance of F···H Interaction towards High-Performance Blue Phosphorescent OLEDs with EQE over 33%. *Angew. Chem., Int. Ed.* **2025**, *64*, 7.
(29) Hang, X. C.; Fleetham, T.; Turner, E.; Brooks, J.; Li, J. Highly Efficient Blue-Emitting Cyclometalated Platinum(II) Complexes by Judicious Molecular Design. *Angew. Chem., Int. Ed.* **2013**, *52*, 6753−6756.
(30) Li, G. J.; Liu, S.; Sun, Y. L.; Lou, W. W.; Yang, Y. F.; She, Y. B. N-Heterocyclic carbene-based tetradentate platinum(ii) complexes for phosphorescent OLEDs with high brightness. *Journal of Materials Chemistry C* **2021**, *10*, 210−218.
(31) Li, G. J.; Wolfe, A.; Brooks, J.; Zhu, Z. Q.; Li, J. Modifying Emission Spectral Bandwidth of Phosphorescent Platinum(II) Complexes Through Synthetic Control. *Inorg. Chem.* **2017**, *56*, 8244−8256.
(32) Luo, Y. F.; Tang, L. K.; Zeng, W. R.; Chen, Z. Z.; Xu, Z. G.; Zhang, Y. C.; Yang, Y.; Hu, J. P.; Tang, D. Y. Influence of coordinate character on the photo-deactivate process for Pt(II) complex: A theoretical investigation. *Opt. Mater.* **2024**, *153*, 115525.
(33) Osipov, A.; Kim, I.; Odinokov, A.; Son, W. J.; Yakubovich, A. V.; Choi, H. Tetradentate Pt(II) Phosphors: A Computational Analysis of Nonradiative Decay Rates and Luminescence Efficiency. *J. Phys. Chem. C* **2020**, *124*, 12039−12048.
(34) Luo, Y. F.; Xu, Y. Y.; Zhang, W. T.; Li, W. Q.; Li, M.; He, R. X.; Shen, W. Theoretical Insights into the Phosphorescence Quantum Yields of Cyclometalated (C***C*) Platinum(II) NHC Complexes: $\pi$ -Conjugation Controls the Radiative and Nonradiative Decay Processes. *J. Phys. Chem. C* **2016**, *120*, 3462−3471.
(35) Feng, T. T.; Bai, F. Q.; Xie, L. M.; Tang, Y.; Zhang, H. X. Theoretical study and design of highly efficient platinum(II) complexes bearing tetradentate ligands for OLED. *Rsc Advances* **2016**, *6*, 11648−11656.
(36) Luo, Y. F.; Xu, Y. Y.; Zhang, W. T.; Li, M.; He, R. X.; Shen, W. Exploring the Photodeactivation Pathways of Pt ONCN Complexes: A Theoretical Perspective. *ChemPhysChem* **2016**, *17*, 69−77.
(37) Xu, Y. Y.; Luo, Y. F.; Li, M.; He, R. X.; Shen, W. Theoretical Insights into the Photo-Deactivation of Emitting Triplet Excited State of (CN)Pt(OO) Complexes: Radiative and Nonradiative Decay Processes. *J. Phys. Chem. A* **2016**, *120*, 6813−6821.
(38) Zhang, F. Y.; Xu, Y. Y.; Zhang, W. T.; Shen, W.; Li, M.; He, R. X. Theoretical Studies of Photodeactivation Pathways of NHC-Chelate Pt(II) Compounds with Different Numbers of Triarylboron Units: Radiative and Nonradiative Decay Processes. *J. Phys. Chem. A* **2017**, *121*, 690−698.
(39) Chen, X.; Deng, S. H.; Zhang, W. J.; Yin, P. A.; Li, W. T.; Shuai, Z. G. First-Principles Prediction for Phosphorescence Spectra of Tetradentate Platinum(II) Complexes with Narrow Emission Width. *J. Phys. Chem. A* **2025**, *129*, 2493−2509.
(40) Tao, J. M.; Perdew, J. P.; Staroverov, V. N.; Scuseria, G. E. Climbing the density functional ladder: Nonempirical meta-generalized gradient approximation designed for molecules and solids. *Phys. Rev. Lett.* **2003**, *91*, 4.
(41) Staroverov, V. N.; Scuseria, G. E.; Tao, J. M.; Perdew, J. P. Comparative assessment of a new nonempirical density functional: Molecules and hydrogen-bonded complexes. *J. Chem. Phys.* **2003**, *119*, 12129−12137.
(42) Goerigk, L.; Grimme, S. A thorough benchmark of density functional methods for general main group thermochemistry, kinetics, and noncovalent interactions. *Phys. Chem. Chem. Phys.* **2011**, *13*, 6670−6688.
(43) Weigend, F. Accurate Coulomb-fitting basis sets for H to Rn. *Phys. Chem. Chem. Phys.* **2006**, *8*, 1057−1065.
(44) Weigend, F.; Ahlrichs, R. Balanced basis sets of split valence, triple zeta valence and quadruple zeta valence quality for H to Rn: Design and assessment of accuracy. *Phys. Chem. Chem. Phys.* **2005**, *7*, 3297−3305.
(45) Frisch, M. J.; et al. *Gaussian 16, Revision B.01*; Gaussian, Inc.: Wallingford, CT, 2016.
(46) Neese, F. Software update: The ORCA program system—Version 5.0. *Wiley Interdisciplinary Reviews-Computational Molecular Science* **2022**, *12*, 15.
(47) Lu, T.; Chen, F. W. Multiwfn: A multifunctional wavefunction analyzer. *J. Comput. Chem.* **2012**, *33*, 580−592.
(48) Eyring, H. The activated complex in chemical reactions. *J. Chem. Phys.* **1935**, *3*, 107−115.
(49) Wang, Y.; Peng, Q.; Shuai, Z. G. A computational scheme for evaluating the phosphorescence quantum efficiency: applied to blue-emitting tetradentate Pt(ii) complexes. *Materials Horizons* **2022**, *9*, 334−341.
(50) Niu, Y.; Peng, Q.; Shuai, Z. Promoting-mode free formalism for excited state radiationless decay process with Duschinsky rotation effect. *Science in China Series B-Chemistry* **2008**, *51*, 1153−1158.
(51) Niu, Y. L.; Li, W. Q.; Peng, Q.; Geng, H.; Yi, Y. P.; Wang, L. J.; Nan, G. J.; Wang, D.; Shuai, Z. G. MOlecular MAterials Property Prediction Package (MOMAP) 1.0: a software package for predicting the luminescent properties and mobility of organic functional materials. *Mol. Phys.* **2018**, *116*, 1078−1090.
(52) Peng, Q.; Yi, Y. P.; Shuai, Z. G.; Shao, J. S. Toward quantitative prediction of molecular fluorescence quantum efficiency: Role of Duschinsky rotation. *J. Am. Chem. Soc.* **2007**, *129*, 9333−9339.
(53) Shuai, Z. G. Thermal Vibration Correlation Function Formalism for Molecular Excited State Decay Rates. *Chin. J. Chem.* **2020**, *38*, 1223−1232.
(54) Du, J. H.; Luo, Y. F.; Xie, X. H.; Hu, W. H.; Shen, W. Tuning the electronic and photophysical properties of platinum(II) complexes through ancillary ligand modification: a theoretical study. *Mol. Simul.* **2016**, *42*, 1035−1041.
(55) Luo, Y. F.; Guo, Y.; Shou, X. C.; Chen, Z. Z.; Xu, Z. G.; Tang, D. Y. Investigate the Relationship between Structure and Triplet Potential Energy Surface to Control the Phosphorescence Quantum Yield of Platinum(II) Complex: A Theoretical Investigation. *Inorg. Chem.* **2022**, *61*, 9162−9172.
(56) Yan, X.; Li, W. Q.; Zhang, H. Z.; Cai, W. L.; Wang, J.; Shen, W. DFT/TDDFT insight into the impact of ring size of the NHC chelating unit of high effective phosphorescent Platinum (II) complexes. *Appl. Organomet. Chem.* **2018**, *32*, 11.

Downloaded from pubs.acs.org/jpclcd/article-pdf/17/43/12289/6888372/acs.jpclett.6c03198.pdf by CHINESE UNIV OF HONG KONG SHENZHEN user on 02 November 2026


https://doi.org/10.1021/acs.jpclett.6c03198
J. Phys. Chem. Lett. 2026, 17, 12289−12296

(57) Wu, Z. X.; et al. Theoretical insight into the photodeactivation pathway of the tetradentate Pt(II) complex with different inductive substituents. *Appl. Organomet. Chem.* **2019**, *33*, 12.
(58) Gao, J. X.; Shi, X. D.; Luo, Y. F.; Zhang, Z. L.; Wang, Y. T.; Liang, L.; He, G.; Liu, W.; Tang, D. Y.; Hu, J. P. A promising strategy for increasing phosphorescent quantum yield: The ligand 10-cyclic chelate of the tetradentate Pt(II) complex. *Appl. Organomet. Chem.* **2022**, *36*, 12.
(59) Kim, Y.; Kim, J.; Kim, W. Y. Engineering Excited States of Pt-Based Deep-Blue Phosphors to Enhance OLED Stability. *Acs Omega* **2025**, *10*, 56753−56762.
(60) Zuo, K.; Luo, Y. F.; Sun, X.; Shen, W.; Tang, D. Y.; Hu, J. P. Theoretical insight into the photodeactivation pathway of the tetradentate Pt(II) complex: The $\pi$-conjugation effect. *Appl. Organomet. Chem.* **2018**, *32*, 10.
(61) Endo, A.; Sato, K.; Yoshimura, K.; Kai, T.; Kawada, A.; Miyazaki, H.; Adachi, C. Efficient up-conversion of triplet excitons into a singlet state and its application for organic light emitting diodes. *Appl. Phys. Lett.* **2011**, *98*, 3.
(62) Goushi, K.; Yoshida, K.; Sato, K.; Adachi, C. Organic light-emitting diodes employing efficient reverse intersystem crossing for triplet-to-singlet state conversion. *Nat. Photonics* **2012**, *6*, 253−258.

Downloaded from pubs.acs.org/jpclcd/article-pdf/17/43/12289/6888372/acs.jpclett.6c03198.pdf by CHINESE UNIV OF HONG KONG SHENZHEN user on 02 November 2026



https://doi.org/10.1021/acs.jpclett.6c03198
*J. Phys. Chem. Lett.* 2026, 17, 12289−12296